Advanced Materials

～夢をかたちに～

新素材 ニュース

CRDAM Newsletter

共同研究開発センター

Vol.6
2015.11

CONTENTS

東北大学　金属材料研究所　附属新素材共同研究開発センター

Cooperative Research and Development Center for Advanced Materials, IMR, Tohoku University

活動報告

片平まつり２０１５　きんけん一般公開　に出展・展示

平成２７年１０月１０日、１１日の二日間にわたって片平まつり２０１５きんけん一般公開「きんけん宝島～みんなで探検キッズラボ～」が開催されました。
片平まつりは、１９９８年からほぼ隔年で開催し、今回で９回目となります。今回は、これまでで最多の１１の研究所等が参加しました。
金研では、各研究室、センターが企画した３０以上のイベントブースが用意され、朝から多くの来場者でにぎわいました。
当センターでは、「動くかな？磁力の不思議！」と題し、３種類のコイルを使っておもちゃの新幹線を動かすクイズや、銅の重さを予想して当てるクイズも行い、正解者にはくじ引きでエコウォーマーを配布し、大勢の子どもたちが楽しそうに参加していました。
金研全体では、前回を１，０００人ほど上回る５，２０１人の来場者があり、二日間とも大盛況となりました。

コイルクイズ

重さクイズ

活動報告

ニューヨーク州立大学ビンガムトン校　上級研究員 Bae In-Tae　先生による講演会開催

平成27年5月22日(金)、国際教育研究棟2階セミナールームⅠにおいて、ニューヨーク州立大学ビンハムトン校上級研究員で、新素材共同研究開発センター客員准教授のBae In-Tae先生による講演会を開催しました。演題は“Comprehensive crystal structure analysis for $BiFeO_3$ thin film using transmission electron microscopy”で、近年マルチフェロイック材料として注目を集めている$BiFeO_3$薄膜の透過電子顕微鏡による微細構造解析に関するものでした。講演では特に、Bae先生らが近年見出した極薄領域における新奇な強誘電特性と薄膜の原子的構造についてお話しされました。本講演会は応用物理学会東北支部との協賛ということもあり、金研のみならずWPIや工学研究科からもご参加頂き、当日は20名を超える盛況となりました。講演終了後、会場からは薄膜の原子的構造と強誘電特性について種々の質問が飛び交い、活発な議論がなされ、改めてマルチフェロイック材料に関する注目度とともに、電子線構造解析への関心の高さを窺わせる結果となりました。

なお、Bae先生は約1ヶ月間の金研滞在中に透過電子顕微鏡観察を中心に多くの新しい実験結果を得て、6月12日に帰国されました。

退職者挨拶

准教授　佐藤　和久

このたび10月1日付で大阪大学超高圧電子顕微鏡センターに異動することとなりました。金研では平成19年10月以来、今野研に6年8ヶ月、新素材共同研究開発センターに1年４ヶ月、合計８年間にわたりお世話になりました。この間、今野豊彦教授、牧野彰宏教授、古原忠教授をはじめ本所の諸先生方にご指導頂き大変お世話になりました。ここに深く感謝申し上げます。また、多くの諸先輩方や同僚にも恵まれ、たくさんのことを学び大変充実した日々を過ごすことができました。新素材センターでは、短い期間ではありましたが、センター教員、技術職員、事務職員の皆様に日々支えられながら、何とか日常の業務をこなすことができました。センター教職員の皆様に厚くお礼申し上げます。センター着任当初、大型の材料合成装置や高性能な分析装置群が日々共同利用研究に供されている様子を目の当たりにして、圧倒されたことを覚えております。このように大変恵まれた環境に身を置くことができましたことは、私の人生においてかけがえのない財産となりました。その一方で、年間100件にも上る共同利用研究に十分貢献できなかったことと、高度な装置群を存分に活用させて頂く前に異動することとなったことが心残りです。最後になりましたが、金研ならびに新素材センターの益々のご発展を祈念しますとともに、今後ともご指導ご鞭撻のほどどうぞよろしくお願い申し上げます。有難うございました。

平成２７年度客員教員（国外）研究成果報告

Development of Novel Scintillating and Other Crystals

Valery TCHANI (CHANI)

Svetcha, Canada

This report accumulates research activities performed during my three-month visit to IMR, Tohoku University from April 1 to June 30, 2015. In the past, I had experience to work in IMR either as staff member or visiting researcher.

General goal of the visit was participation in research projects associated with new material conceptions in the field of scintillating and other single-crystalline substances that have potential of commercial success for numerous industrial applications. The results are summarized below.

1. Eu-Doped SrI_2 Crystals. Growth of 2-inch diameter macro-defect-free SrI_2 crystals by the vertical Bridgman method was examined. The crystals were produced using apparatus similar to that designed for the micro-pulling-down (μ-PD) process (Fig.1). The growth system had removable and well-isolated growth chamber made of quarts glass ampoule. Thus, fabrication of highly hydroscopic materials became possible.

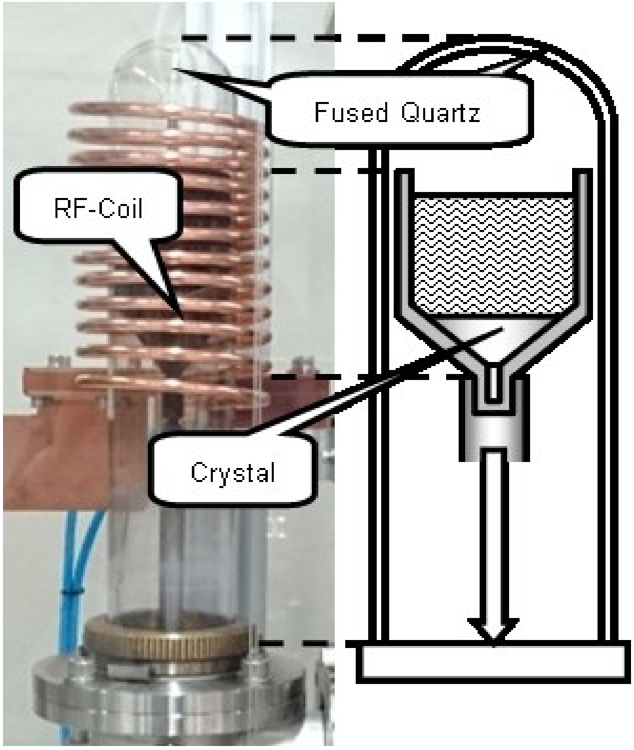

Fig.1. SrI_2 growth by Bridgman method

Bubble- and crack-formation was detected in the crystals produced at the initial stage of the experiments as typical defects. The amount of the bubbles captured by the crystals was reduced considerably after preliminary vacuum degassing. Number of cracks appeared in the as grown crystals was not reduced significantly after modification of the crucible shape and reducing the cone angle of the bottom of the crucible from 90° to 70°. However, decrease of the temperature of the melt at initial stage of the growths with corresponding elimination of seed over-melting and slow cooling of the as grown crystals resulted formation of macro-defect freeEu:SrI_2 crystals (Fig.2).

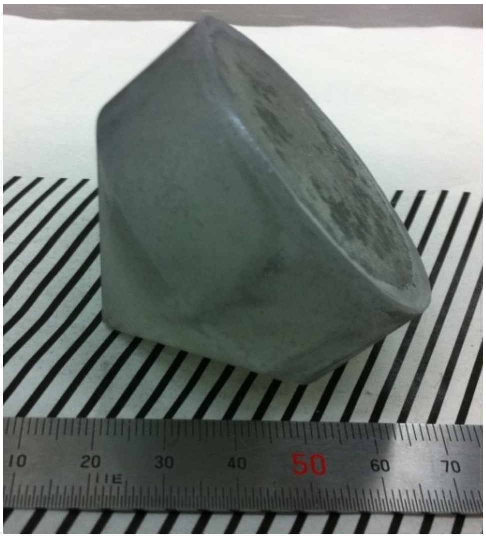

Fig.2. 2-inch crack-free Eu:SrI_2 crystal

2. Ce-Doped $(La,Gd)_2Si_2O_7$ (LGPS) Crystals. Growth of 2-inch diameter LGPS crystals by Czochralski method was studied. The best growth results were observed for the CZ crystals produced from the melt of about $La_{0.5}Gd_{1.5}Si_2O_7$ composition. This composition represents only host material without consideration of the Ce-dopant content. This composition is also in good agreement with chemical formula of [RE1][RE2][RE3][RE4]Si_4O_{14} introduced in the past to reflect four types of rare-earth [RE] crystallographic sites detected in pyrosilicates with triclinic structure. Following the above formula, the composition of $La_{0.5}Gd_{1.5}Si_2O_7$ can be easily transformed to $LaGd_3Si_4O_{14}$ assuming that La^{3+} cations occupy unique [RE] crystallographic sites. This formula represents ideal distribution of RE-cations between crystallographic sites of LGPS structure. However, in real world, anti-site defects are often observed. Thus, some part of La^{3+} may occupy Gd-sites and vice versa. These cross-substitutions were not well studied in the LGPS structure and are not considered in this report. Thus, at the moment, the $LaGd_3Si_4O_{14}$ quasi-stoichiometric composition was confirmed to be most favorable one regarding crystal growth results. The Ce:LGPS crystals produced from the melts of approximately

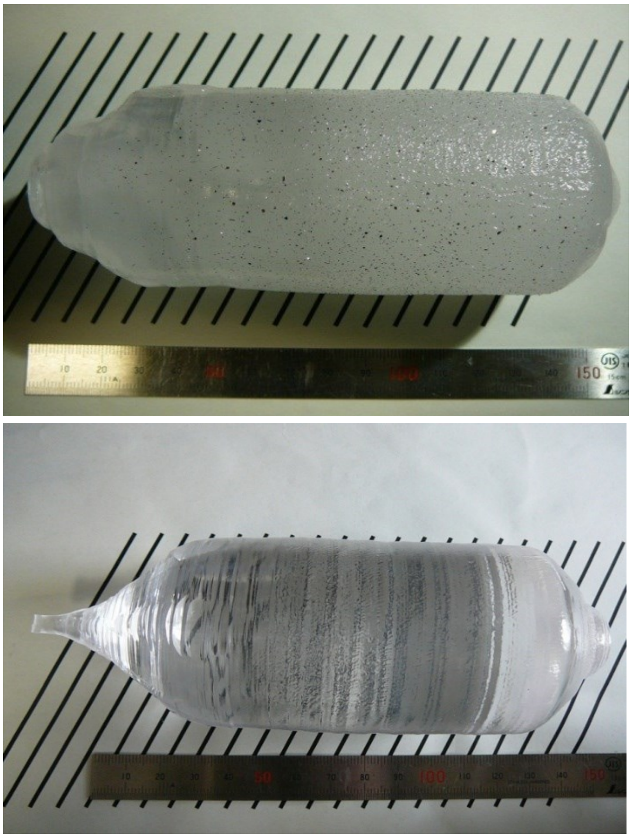

Fig.3. 2-inch Ce:LGPS crystals produced before(top) and after (bottom) process optimization.

The seed rotation rate ranged from 3 to 10 rpm. Two types of seed rotation management were examined. At some growths, the rotation rate was fixed to be constant. However, in the most of the processes, the rotation rate was modified just after starting of body (cylindrical) part of the crystal (Fig.4) to correct forced convection, melt flow pattern, temperature distribution, and shape of the solid-liquid interface. In such cases, the rotation was continuously reduced during the body growth and fixed again when decrease of the crystal diameter was started to establish “tail” part of the crystals as it is illustrated in Fig.4.

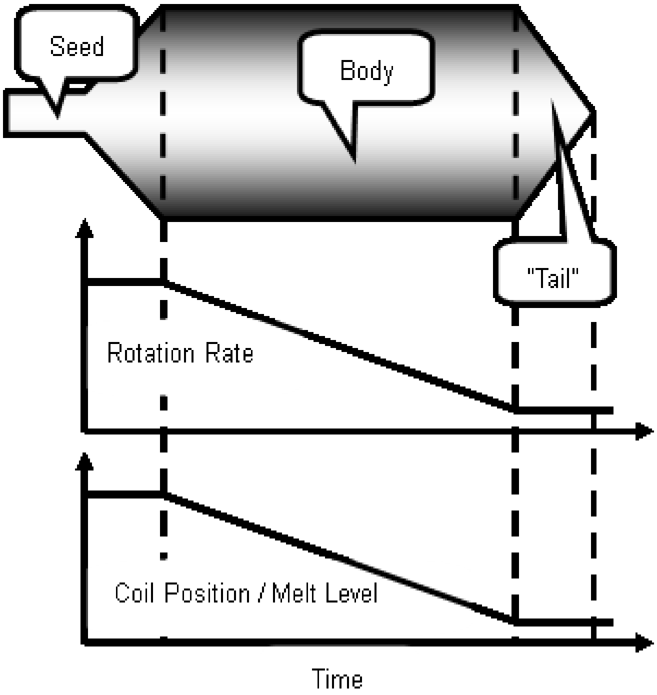

Fig.4. Rotation rate and inductive coil position adjustment schedule.

The position of the RF coil was not always fixed. In most of the processes, its position continuously reduced also starting from the moment when growth of body part began (Fig.4). Thus, the position of the top of the coil was continuously adjusted to be in the same level (height) as the level of the melt remained in the crucible during the whole body part growth. It is evident that the melt level drops when crystal growth is progressed. As a result of this drop, the temperature distribution and thermal gradients at vicinity of the growth interface changes. To compensate this change the position of the RF coil was also corrected according to Fig.4.

The hot zone was in most cases equipped with iridium after-heater also required for improvement of thermal gradient conditions.

2. $Ca_3Ta(Ga,Al)_3Si_2O_{14}$ Crystals. 2-inch diameter macro-defect-free $Ca_3Ta(Ga,Al)_3Si_2O_{14}$ crystal growth by Czochralski method was optimized. Prototype langasite type crystal of $Ca_3TaGa_3Si_2O_{14}$ (CTGS) is well-known. However, this material contains Ga_2O_3 as one of the major ingredients that is expensive. Therefore, the idea to substitute at least part of Ga^{3+} with isovalent Al^{3+} in the CTGS structure motivated growth of $Ca_3Ta(Ga,Al)_3Si_2O_{14}$ (CTGAS) mixed crystals.

The process developed resulted fabrication of CTGS crystals of reasonable structural and optical quality (Fig.5).

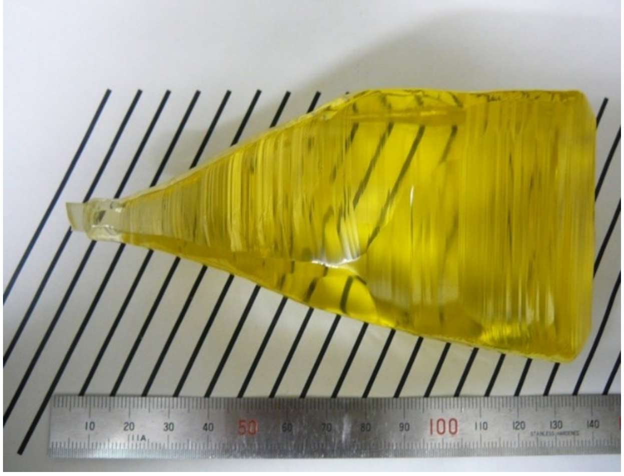

Fig.5. 2-inch $Ca_3TaGa_{1.5}Al_{1.5}Si_2O_{14}$ crystal

According to preliminary results, the melting points of the $Ca_3TaGa_3Si_2O_{14}$ and $Ca_3TaAl_3Si_2O_{14}$ end member compounds of $Ca_3TaGa_{1.5}Al_{1.5}Si_2O_{14}$ crystal are similar. Therefore, segregation between Ga^{3+} and Al^{3+} competing cations is negligible.

Acknowledgments

I would like to thank all the members of Yoshikawa Laboratory and other departments of IMR for their kind assistance and help.

1. A. Yoshikawa, Y. Shoji, Y. Yokota, S. Kurosawa, S. Hayasaka, V. I. Chani, T. Ito, K. Kamada, Y. Ohashi, V. Kochurikhin, Czochralski Growth of 2 Inch Eu-Doped SrI_2 Single Crystals for Scintillator Applications, to be submitted to Crystal Growth and Design.

2. A. Yoshikawa, S. Kurosawa, Y. Shoji, V. I. Chani, R. Murakami, K. Kamada, Y. Yokota, Y. Ohashi, V. Kochurikhin, Czochralski Growth of 2 Inch Ce-Doped $(La,Gd)_2Si_2O_7$ for Scintillator Application, to be submitted to Journal of Crystal Growth.

3. A. Yoshikawa, Y. Shoji, Y. Ohashi, Y. Yokota, V. I. Chani, M. Kitahara, T. Kudo, K. Kamada, S. Kurosawa, A. Medvedev, V. Kochurikhin, Czochralski Growth of 2 Inch $Ca_3Ta(Ga,Al)_3Si_2O_{14}$ Single Crystals for Piezoelectric Applications, to be submitted to Journal of Crystal Growth.

4. A. Yoshikawa, S. Kurosawa, K. Kamada, J. Pejhal, Y. Yokota, Y. Ohashi, V. I. Chani, M. Nikl, A. Ito, T. Goto, G. Boulon, Recent development of ceramics and single crystals for scintillator application, to be submitted to Radiation Measurements/

Keywords: crystal growth, scintillator

E-mail: vchani@gmail.com

Resonant Raman spectra of atomically precise CdSe nanoclusters of extremely small size: experiment and first principles calculation

Prof. Igor Dmitruk

National Taras Shevchenko University of Kyiv, Ukraine

From 1^{st} of June to 31^{st} of July 2015 I worked as a visiting professor in the Cooperative Research and Development Center for Advanced Materials at the Institute of Materials Research, Tohoku University working with Associate Professor Rodion Belosludov. During this visit I have worked on the problem of structure determination of CdSe nanoclusters having extremely small size. Two methods have been applied: resonant Raman spectroscopy and first-principles calculations.

For nanoclusters (NCs) of sizes less than 2 nm, n is typically less than a hundred and most of them reside at the surface. Such small nanoclusters exhibit quantum confinement energy comparable to the binding energy. Characteristic feature of these nanoclusters and indication of their unique properties is existence of so-called "magic" numbers – numbers of atoms or molecules forming clusters with elevated stability at atomic precision. Examples of series of magic numbers are well known for carbon fullerenes (20, 36, 60, 70, 80, 84, …), alkali metals (2, 8, 20, 40, …), noble metals and inert gases (4, 13, 55, …) and predicted also for closed shells of binary compounds like BN (12, 16, 28, 36, 52, …).

Recently we have found a novel series of magic nanoclusters for II-VI compounds: 13, 19, 33, 34, and 48. For the case of CdSe $(CdSe)_{33}$ and $(CdSe)_{34}$ magic nanoclusters have been prepared in macroscopic quantities. Surprisingly, ten years of research and availability of the substance in desired quantity had not led to unambiguous determination of the structure of these magic nanoclusters. Because of extremely small size of less than 2 nm, single cluster does not give definitive structure information in diffraction measurement. Furthermore, the clusters are covered with loosely attached surfactant molecules in unknown quantity and chemical states. That precludes preparation of a high-quality single cluster crystal for XRD structure determination. Other known structure-sensitive techniques, like EXAFS or NMR provide only local information which helps a little in decoding atomic arrangement in a whole particle.

Taking into account these considerations we turn attention to Raman scattering as a well-known structure-sensitive phenomenon. Of course, it does not allow solving the inverse problem of structure determination, but it allows to check any suggestions of possible structure of nanoclusters. Raman spectroscopy is a useful tool for investigating NPs because, Raman spectrum provides information on bonding character and symmetry of atomic arrangement and it is not sensitive to local defects (unlike photoluminescence, for example).

Full geometry optimization and vibrational and electronic spectra analyses of CdSe nanoclusters have been performed using density functional theory (DFT) with B3LYP exchange correlation functional and DGDZVP basis set. Time-dependent DFT (TDDFT) has been applied for electronic excited states calculations.

Main spectroscopic feature of semiconductor nanoparticles is their strong excitonic absorption peak, which demonstrates well-known quantum size effect – blue shift with particle size decreases. Our magic CdSe nanoparticles have intense excitonic transition at approx. 3 eV in absorption spectrum (see Fig.1). It is very narrow (0.11 eV) comparing to typical CdSe nanoparticles with crystalline structure since for the sample consisting of only magic nanoclusters there is no broadening caused by size distribution.

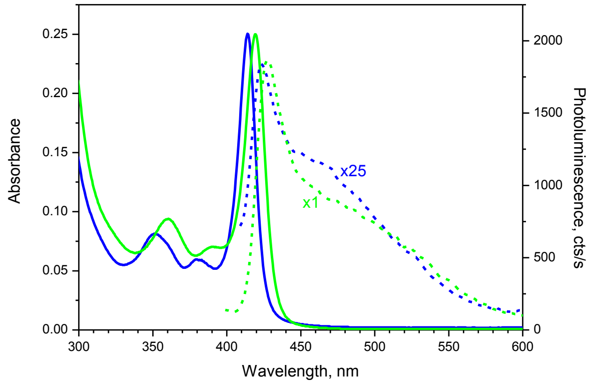

Fig. 1. Absorption (solid) and photoluminescence (dash) spectra of magic CdSe nanoclusters covered with octylamine in toluene (blue) and covered with cysteine in water (green).

Figure 2 shows the Raman spectrum on truly uni-sized CdSe NCs measured for the first time, as confirmed by mass spectrometry. It consists of several characteristic features: a broad first order band consisting of two components at 194 cm^{-1} and 183 cm^{-1}, and small, broad low energy features below 120 cm^{-1}. Spectra of toluene grown amine-stabilized NCs and water-based cysteine stabilized NCs differ only in details: ratio of intensities of the components of fine structure of main 200 cm^{-1} band and spectral positions of low-frequency bands (see Fig. 2). These changes can be attributed to the influence of different capping surfactant molecules.

These spectra were observed only if the wavelength of incident laser beam was chosen as 413.1 nm Kr^+ line that falls within exciton absorption band for both toluene and water soluble samples. Thus, it is a case of resonant Raman scattering.

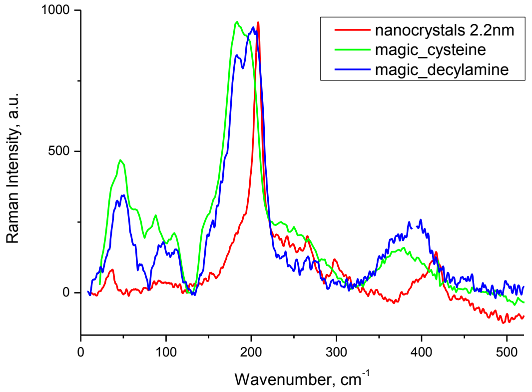

Fig. 2. Raman spectra of CdSe magic nanoclusters and nanocrystals.

To investigate Raman spectral profiles expected in nanoclusters of sizes less than 2 nm, first-principle molecular dynamics calculations were performed on two representative structure models of $(CdSe)_n$ nanoclusters. One is a closed shell structure that we proposed previously for $(CdSe)_{33}$ and $(CdSe)_{34}$ [published in Nature Materials, 2004]. According to mass-spectrometry data, studied samples contained a mixture of $(CdSe)_{33}$ and $(CdSe)_{34}$ in approximately equal quantities. The most stable structure suggested for $(CdSe)_{34}$ is core-cage consisting of an empty shell $(CdSe)_{28}$ enclosing hexagonal prism core, $(CdSe)_6$. For $(CdSe)_{33}$ initially was suggested similar core-cage structure of $(CdSe)_{28}$ shell with small cluster $(CdSe)_5$ inside. But later another possible structure was found: $(CdSe)_{30}$ cage enclosing hexagon $(CdSe)_3$. These two structures have almost equal binding energies, and the difference can be smaller than accuracy of computational method.

The other model is a cutting piece of bulk wurtzite or zinc blend crystal of less than 2 nm in size with full geometry optimization of the lattice. This is the bulk fragment model confirmed by diffraction measurements for sizes larger than 2nm, and adopted in Raman spectra reported in a number of papers. We first use DFT methods instead of pure Hartree-Fock, because they are less time-consuming and can provide acceptable results both for vibrational and electronic spectra. Second, we neglected influence of surfactant molecules and performed all calculations with bare CdSe NCs. The reason for this simplification is similarity of Raman and nearly identical optical absorption spectra for NCs with different surfactants and in different solvents that indicates small influence of surfactant and solvent on electronic and vibrational spectra.

In a bulk crystal having translational symmetry, lattice vibrations consist of low energy acoustic phonon and high energy optical phonon separated by a phonon gap in their dispersion curves. If the crystal has a finite size, standing waves of both acoustic and optical phonons reflected at the crystal boundaries are also excited. At the boundaries, surface vibrations are excited as well at energies located mainly in the phonon gap. In addition, mode mixings take place between these vibrations. These vibrational modes, therefore, are sensitive to not just the size but to the boundary structure, and these mode increase makes vibrational spectrum resemble vibrational DOS. As the size is reduced below 2nm of molecular like nanoclusters, more than half of constituent atoms are at the surface that substantial atomic rearrangement takes place together in the entire nanocluster for stable configuration, leading to magic number *n*. Resultant stable geometry and atomic arrangement can be depicted in vibrational spectrum.

Characteristic feature of experimental Raman spectra of magic CdSe nanoclusters is a dip around 130 cm^{-1}. In calculated DOS of all suggested structures, a gap is present at approximately equal frequency (Fig. 3a). It should be pointed out that nanoparticles with the structure of bulk fragments have no dip in vibrational DOS (Fig. 4b). From the results discussed above we can conclude that a gap in vibrational DOS spectrum is characteristic feature of our model of close shell structures. Following is a crude explanation: in a molecular picture, two kinds of vibrations can exist in closed shell with substantially different frequencies – stretching of the mesh of bonds and shell bending. In a solid picture, optical and acoustic vibrations of both bulk and surface modes are not so strongly mixed or broadened in the shell structure to be separately distributed in the DOS compared with nearly overlapped in the DOS of tiny crystalline fragments of less symmetric surface geometry.

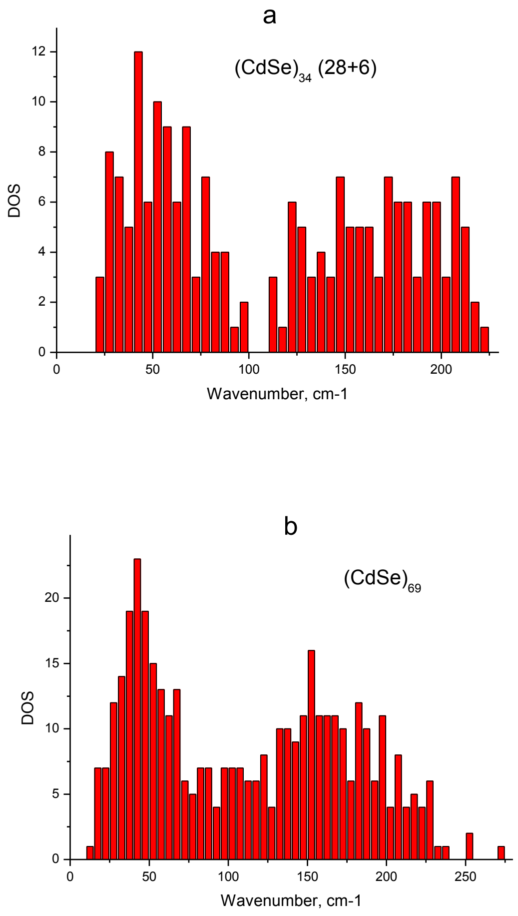

Fig. 3. DOS of vibrational states of core-cage cluster (a) and bulk fragment (b).

Many previous Raman measurements on semiconductor NPs show strong influence on the spectral profile by resonant electronic transitions. This influence leads to dramatic changes of selection rules and intensity profile. Spectral manifestations of this influence are the following: i) large number and intensity of overtones, ii) efficient excitation of Raman spectrum only if excitation wavelength is within exciton absorption peak, iii) in the case of nanocrystals the dominant line corresponds to LO phonon which is forbidden for the case of conventional non-resonant Raman.

There are a number of papers that address problem of resonant Raman on molecules. Two approaches are the most popular: sum on the multiple states, and analysis of the equilibrium geometry of excited state. Both are well developed and have been successfully demonstrated with the first-principles calculations. However, a few papers that deal with resonant Raman on semiconductor nanoparticles are based on molecular dynamics of crystalline lattice and some assumption about electric field generated by electron-hole pair confined in nanoparticle.

The case of magic CdSe NCs is just in between of molecule and crystalline lattice. And hopefully, analysis of this case can bridge the gap between molecular and crystalline approaches. At first, Raman intensities were calculated from Raman activities with the standard formula. Then Raman spectra are calculated as a convolution of Raman intensities of all modes. The calculations have been performed for predicted structures of magic $(CdSe)_{33}$ and $(CdSe)_{34}$ nanoclusters. Calculated resonant Raman spectra of magic CdSe nanoclusters (see Fig. 4) and small nanocrystals demonstrate reasonable agreement with experimental ones. These results allow to exclude bulk crystalline fragments as possible structure.

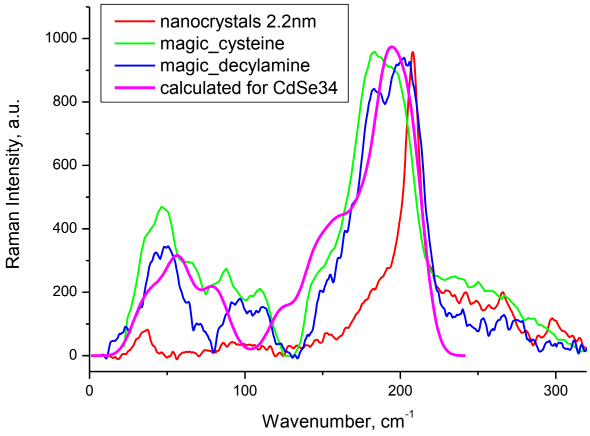

Fig. 4. Calculated resonant Raman spectrum of core-cage $(CdSe)_{34}$ in comparison with experimental spectra of magic nanoclusters.

These clusters can be used as building blocks of novel nanocomposite matherials for applications in nanoelectronics and photonics.

I appreciate invitation to Tohoku University and this unique chance for fruitful collaboration. Many thanks to Director of IMR Prof. Koki Takanashi, Head of Cooperative Research and Development Center for Advanced Materials Prof. Tadashi Furuhara, and my colleague Assoc. Prof. R. Belosludov. I also thankful to Mr. N. Igarashi for continuous support in computer code and facility and Ms. E. Takahashi in her assistance for my family to stay in Sendai.

ありがとう ございました！

Comprehensive transmission electron microscopy study on thin film BiFeO$_3$ grown on (100) SrTiO$_3$

Dr. In-Tae Bae

State University of New York at Binghamton, USA

From 8th of May to 8th of June 2012, I worked as a visiting associate professor in the Shinsozai Center at the Institute of Materials Research (IMR), Tohoku University working with Associate Professor Kazuhisa Sato.

During this visit, I have been focusing on my research of comprehensive crystal structural analysis for thin film BiFeO$_3$ (BFO) grown on single crystalline SrTiO$_3$ (STO) substrates by using aberration (C$_s$) corrected transmission electron microscopies (TEMs) available in IMR of Tohoku University.

BFO is a unique material that possesses multiferroic properties, i.e., ferroelectricity and antiferromagnetism. This implies that BFO has significant application potential for emerging spintronics applications such as multiple-state memory and magnetic random access momory. To date, however, its magnetoelectric response has been known to be too weak to be useful. Recently, it was reported that spontaneous polarization of BFO can be as high as $\sim$60 mC/cm^2 when BFO is hetero-epitaxially grown on STO substrate. In that report, it was argued that lattice stress induced crystal structure alteration (from rhombohedral to tetragonally distorted cubic) is associated with the increase of the spontaneous polarization. Since knowledge about crystal structure of thin film BFO is so critical that a number of follow-up studies have attempted to reveal its crystal structure. While some studies has found BFO crystal structure as pseudo-cubic, others found monoclinically distorted rhombohedral and monoclinic with domain structures. Thus, the crystal structure of thin film BFO remains a topic of debate.

I have recently demonstrated that in order to properly investigate crystal structure of thin film BFO grown on STO, cross-sectional TEM technique along multiple zone axes of STO is highly effective. In particular, [011] zone axis of STO turned out the best zone axis since extra columns of Bragg’s reflection in nano-beam electron diffraction (NBED) pattern for BFO thin films are unmistakably distinctive from that for STO substrate (See Figs. 1(a) and (b)).

- *Extra columns of Bragg’s reflections!*

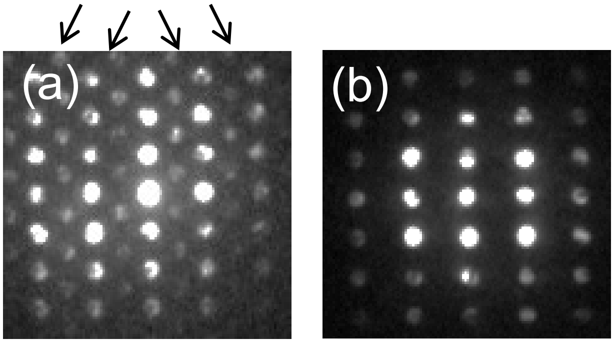

Figure 1 (a) NBED pattern from BFO film that shows extra columns of Bragg’s reflection, and (b) NBED patterns from STO substrate

In order to further investigate the details on crystal structure of thin film BFO as well as its growth mechanism on STO substrate, high resolution TEM image was acquired from 13 nm thick BFO film grown on (100) STO substrate using a C$_s$-corrected TEM with spatial resolution less than 0.1 nm available in IMR of Tohoku University as shown in Fig. 2. The high resolution image turned out to correspond to the atomistic model of [011] zone axis of rhombohedral BFO (see the inset), which is in good agreement with our previous study and further confirm the validity of our crystal structure analysis.

Since local electronic structure of BFO is also important to interpret its physical properties properly, electronic energy loss (EEL) spectra were also acquired from 13nm thick BFO film grown on (100) STO substrate in comparison with bulk BFO material (= 300 nm thick) as exhibited in Fig. 3. The peaks denoted as group 1(1 and 1’) in Figs 3(a) and 3(b) are known to stem from transitions to unoccupied O 2*p* state hybridized with metal, i.e., Fe, 3*d* band. The splitting of peaks into 1 and 1’ was associated with interactions between unoccupied O 2*p* and Bi 5*d* and/or *p* states in BFO. Although the peak 1’ in Fig. 3(b) is not as conspicuous as that in Fig. 3(a), the overall characteristics of group 1 peak are highly similar. In the case of group 2 peaks denoted as 2 and 2’ are attributed to O 2p hybridized with Fe 4s and 4p as well as covalently bonded to Bi states. Although the group 2 peaks in Fig. 3(b) is a bit noisier than that in Fig 3(a), the overall characteristics, i.e., location and shape, are highly similar. Thus, it is speculated that there is no significant electronic structural difference between 13 nm thin BFO and bulk (= 300 nm thick) BFO. This result is in good agreement with the previously mentioned crystal structure analysis result whose conclusion is that both of 13nm and bulk BFOs have identical crystal structure, i.e., rhombohedral.

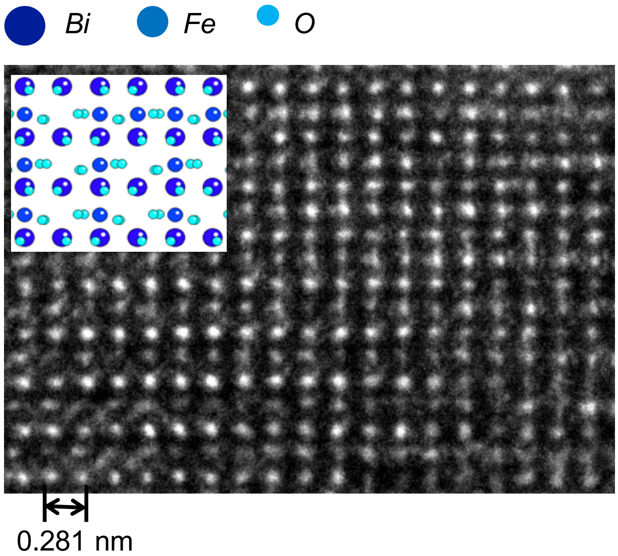

Figure 2 high-resolution TEM image of 13nm thick BFO thin film grown on (100) STO substrate along $[011]_{STO}$ zone axis. Zone axis of BFO corresponds to [211].

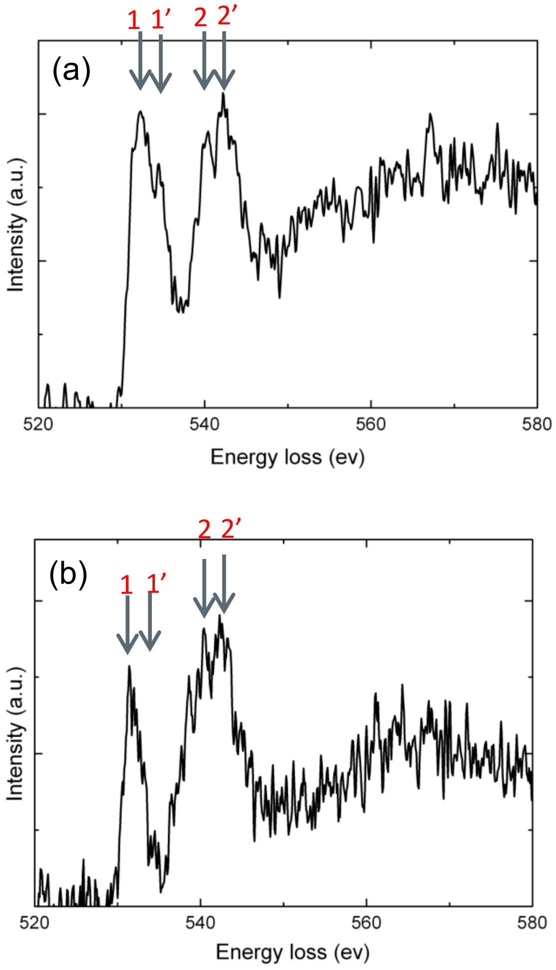

Figure 3 EELS spectra from (a) 13 nm thick BFO film and (b) bulk BFO (300nm thick)

In addition to the data shown in this short report, additional data were obtained for BFO films with much thinner thicknesses of 0.4 and 0.2 nm. The interpretation of those data is currently in progress to put all data together for a peer-review publication.

During the one month of collaboration with Prof. K. Sato and staff members, we have carried out very valuable exploratory experiments that could lead to a solid foundation to understand the underpinning mechanism for the substantial increase of spontaneous polarization in thin film BFO. I would like to deeply express my sincere gratitude to Prof. K. Sato for the invitation to IMR of Tohoku University. I also extend many thanks to Ms. E. Takahashi for helps with the administrative paper works. I wish nothing but all the best for Shinsozai Center and IMR.

Electrochemical properties of Fe-Co-Si-B-P-Cu soft magnetic alloys

Prof. Zhenhua Dan
College of Materials Science and Technology, Nanjing TECH University, China

From 14th of July to 21th of August 2015, I worked as a visiting professor in Cooperative Research and Development Center for Advanced Materials at the Institute of Materials Research, Tohoku University working with Associate Professor Kazuhisa Sato. I already had a working experience at IMR for two years from June 2012 to August 2014.

During this visit, I have been focusing my research on the evaluation of electrochemical properties of Co-substituted Fe-based soft magnetic alloys which have a superior soft magnetic properties and high forming ability. Fe-based nanocrystalline soft magnetic alloys have a high saturation magnetic density and ultralow core loss. They are expected to replace conventional Fe-Si electric steel in future. However, their electrochemical properties have to be investigated extensively in order to precisely predict their reliability, life span and cost control, etc.. Plenty of alloy system have been developed to fulfil some specific requirements for commercial products. Co substitution can improve the saturated magnetic flux density and reduce the coercivity in a viewpoint of soft magnetism. On the other hand, Co substitution can also better the thermal stability, the critical product size of Fe-based amorphous alloys. Fundamental electrochemical aspects of these new alloys need to be clarified and then contribute some positive feedback to alloy design. It has been reported that Co substitution improves the soft magnetic performance of Fe-Si-B-P-Cu alloy and increase the critical size of samples. However, effect of Co substitution on electrochemical properties is still unclear.

The XRD pattern in Fig. 1 shows that the as-spun ribbons have an amorphous state.

Potentiodynamic polarization measurements shows that the amorphous Fe-Co-Si-B-P-Cu samples became better in comparison to the Co-free Fe-Si-B-P-Cu alloys indicating by the positive shift of the open circuit potential and the slight decrease in the passive current density. Surface analysis data obtained by an X-ray photoelectron spectroscope and Auger electron spectroscope in Fig. 2 indicated that the Co element coexisted with iron oxides and the atomic concentration of cobalt oxides gradually increased with the increase of the additive Co contents. The native oxide layer mainly consisted of FeO ($Fe(OH)_2$) and the adsorbed salts.

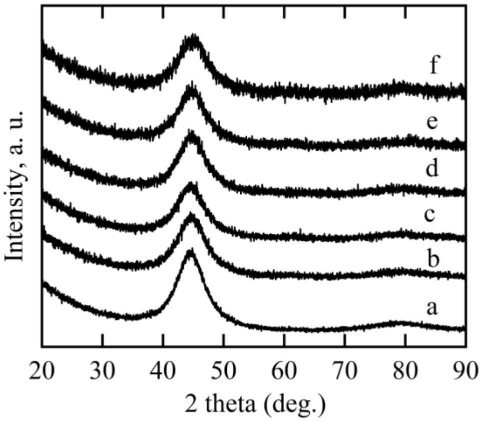

Fig.1. XRD patterns of as-spun Fe-Co-Si-B-P-Cu ribbons; (a) Co-free, (b) -(f): [Co]=1-40at%.

Some cyclic experiments conducted confirmed that the life span of Co-substituted alloys was almost the same as the Co-free alloys in acidic environments. After the CV tests, the residual chemical compounds were confirmed mainly to be composed of FeO ($Fe(OH)_2$), CoO, SiO_2, PO_4^{3-}, and Cu_2O, etc.. The surface morphology in Fig. 3 demonstrated that the different oxidesformed after the cyclic rusting. The flower-like phases are considered to be FeO or $Fe(OH)_2$, and these

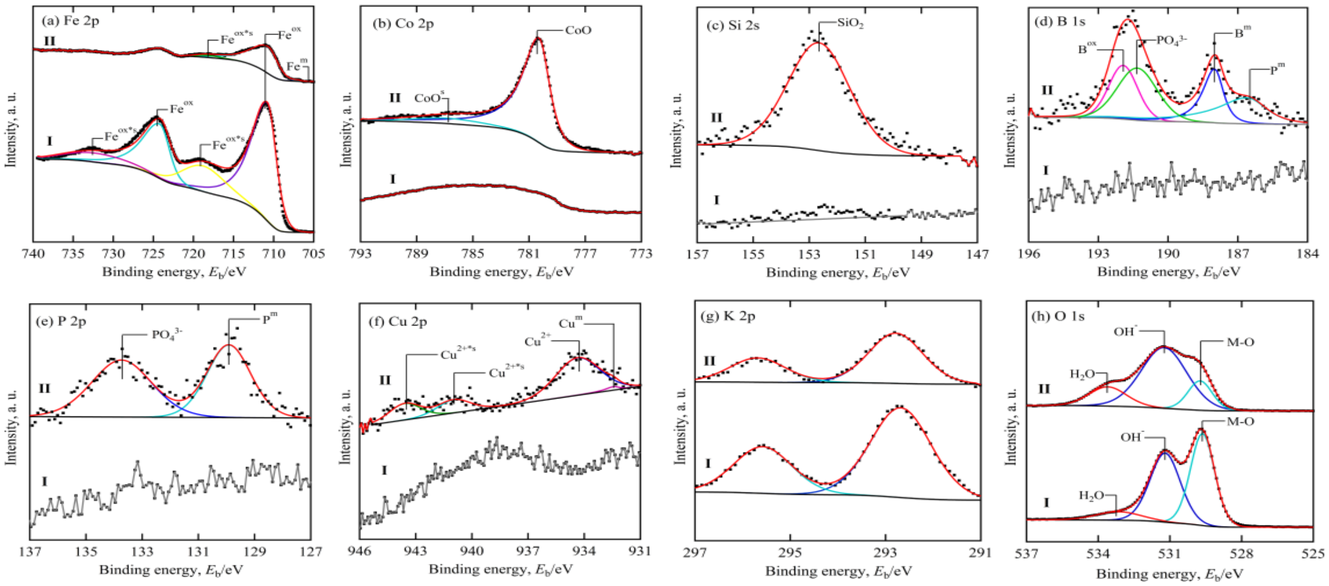

Fig. 2 XPS spectra of Co-substituted alloys before and after CV test.

diamond-shaped particles are likely Co oxides. Therefore, the surface oxides have an ability to act as a catalytic material. With an increase of the cycle numbers, the catalytic ability of the CoO gradually become better. Peak current density increased since the surface became much rougher as shown in Fig. 3 and Fig. 4

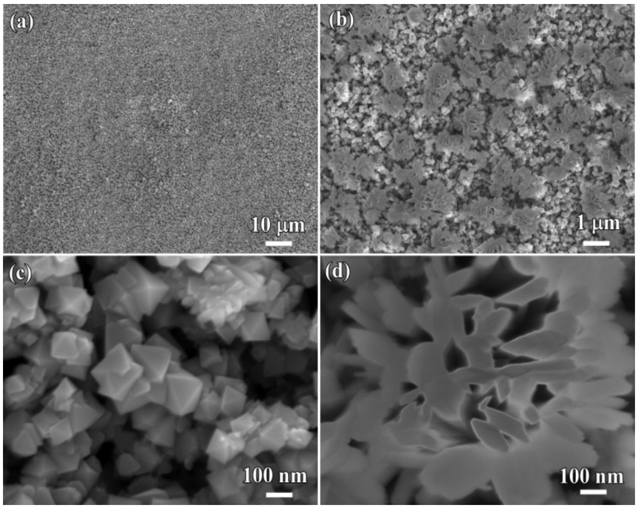

Fig. 3 SEM morphology of Fe-Co-Si-B-P-Cu alloys after 300 cycles of CV tests.

The peak current density of Fe-Co-Si-B-P-Cu alloys is shown in Fig. 4. Fig. 4 indicated that the best Co additive is 4 at% where the maximum catalytic current is appeared at Co%=4at%. The Co content less than 10 at% can make a good performance as a catalyst.

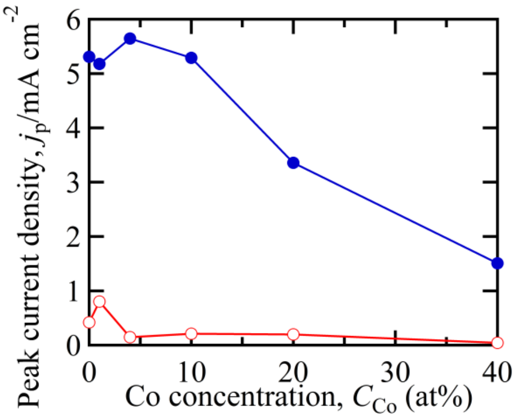

Fig. 4 The peak current density in the first cylce (Red) and 10th cycles (Blue) as a function of the Co content in alloys.

During the one month and half of collaboration with Prof. K. Sato and staff members, we have done some valuable explorations to the electrochemical properties of Co-added alloys by using the advanced apparatus in IMR, Tohoku University. These materials have a great potential for new generation soft magnetic alloys. I would like to express my sincere gratitude to Prof. K. Sato and Prof. A. Makino for the invitation to IMR of Tohoku University. I also extend many thanks to Ms. E. Takahashi for her kind helps with the administrative paper work and very useful daily life advices.

Thank you all again!

Convection Control in Crystal Growth

Prof. Zhong Zeng

Department of Engineering Mechanics, College of Aerospace Engineering, Chongqing University, P.R , China

From July 13, 2015 to August 30, 2015, I worked as a visiting professor to cooperate with Professor Akira Yoshikawa at the Institute of Materials Research (IMR), Tohoku University. In October 1996, I went to IMR for pursuiting my Ph.D. degree, under the supervision of Professor Yoshiyuki Kawazoe, I got my Ph.D. degree in 2000, after 5 years research on fluid dynamics in crystal growth at IMR, and then I went back to China and got a promotion at Chongqing University in 2005. It was my great pleasure to visit IMR again.

During this visit, I focused myself on relieving the dopant segregation of Ce:YAG crystal in improving micro-pulling-down crystal growth technique. Micro-pulling-down, an important method of fiber-shaped crystal growth, is based on the continuous transport of the molten substance through capillary-channel into the crucible bottom. The micro-pulling-down is a cost-effective technique, and a high growth rate (>5mm/min) can be achieved to fabricate fiber-shaped crystals. Therefore, the micro-pulling-down has attracted researcher great attention. So far, semiconductor, oxide and fluoride crystals have been grown successfully by the micro-pulling-down technique.

The configuration of the traditional micro-pulling-down technique is illustrated in Fig. 1, the diameter of capillary-channel is much less than the crystal diameter, which is same size as the shaper, the melt is fed continuously from the micro-channel, and the dominant convection is Marangoni flow, which occurs in local region near free surface. These features result in serious dopant segregation in radial direction for crystal growth with the dopant segregation coefficient k deviating far from 1 (k=0.01 in Ce:YAG, for example).

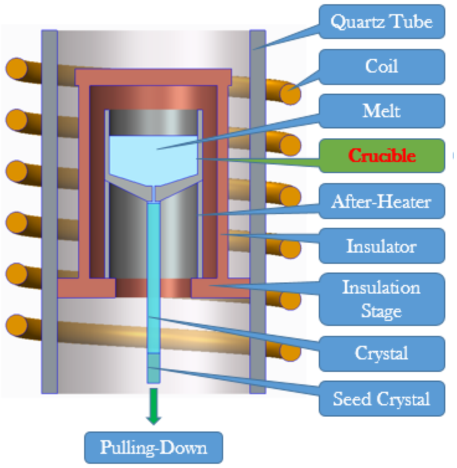

Figure 1: Schematic diagram of adopted micro-pulling down system

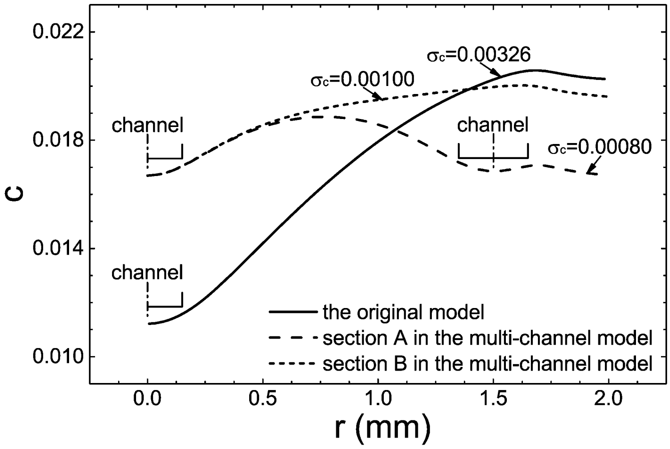

Fig. 2: The radial curves of dopant concentration at the melt-crystal interface of the five-channel and original models. The lines near the word “channel” mark the radial positions of capillary-channels.

To improve the homogeneity of the dopant distribution, the multi-channel crucible, a crucible variant in traditional micro-pulling-down, is adopted, and the optimization on the arrangement of capillary-channels is investigated. Fig.2 indicates that the five-channel crucible is better than the traditional crucible to achieve the dopant homogeneity in radial direction. Based on our investigation numerically, the optimized 9-channel crucible is finally proposed.

各展示室見学・視察一覧

2015　6/5
　株式会社NTTデータ経営研究所　竹内　敬治様　他6名

2015　7/24
　平成27年度戦略的基盤技術高度化支援事業
　「金属ガラス粉末成形による長寿命･高耐食･高強度なミニチュアベアリングの内･外輪生産技術開発」
　 研究開発推進委員会
　ポーライト株式会社　取締役　技術統括部長　羽吹　文夫様　他18名

新素材共同研究開発センターニュースvol.6
2015年11月30日

東北大学　金属材料研究所

附属新素材共同研究開発センター

〒980-8577　仙台市青葉区片平2-1-1
TEL　022-215-2371／FAX　022-215-2137
E-Mail　crdam@imr.tohoku.ac.jp
URL　http://www.crdam.imr.tohoku.ac.jp